Size-dependent particle migration and trapping in three-dimensional microbubble streaming flows

Size-dependent particle migration and trapping in microbubble streaming flows

Andreas Volk[(a)], Massimiliano Rossi[(a)], Bhargav Rallabandi[(b)],
Christian J. Kähler[(a)], Sascha Hilgenfeldt[(c)], Alvaro Marin[(d)†]
[a] *Institute of Fluid Mechanics and Aerodynamics, Bundeswehr University Munich, Neubiberg, Germany*
[b] *Department of Mechanical Engineering, University of California, Riverside, California 92521, USA*
[c] *Department of Mechanical Science and Engineering, University of Illinois, Urbana-Champaign, USA*
[d] *Physics of Fluids, University of Twente, Enschede, The Netherlands.*

Acoustically actuated sessile bubbles can be used as a tool to manipulate microparticles, vesicles and cells. Descriptions of particle positioning have usually invoked simple concepts of radiation forces ("acoustic tweezers"). In this work it is demonstrated experimentally that sessile actuated bubbles positioned at the wall of microfluidic channels induce reproducible particle migration and trapping towards specific spatial positions, with qualitatively different outcomes according to particle size. It is then shown that a quantitative model of particle trajectories is obtained when acknowledging the three-dimensional character of the acoustic streaming flow together with steric exclusion of the particles from confining boundaries. Thus, taking into account 3D flow geometry allows for quantitative prediction and design of particle positioning in a variety of trapping and size-sorting applications.

PACS numbers:

I. INTRODUCTION

The rectification of oscillatory fluid motion into powerful steady flows has been known and understood since the 19th century [1]. In recent years, due to the developments in manipulation of microparticles, micro-organisms and other microscopic objects [2], the research on acoustic rectification, streaming and trapping has been strongly revitalized [3].

Leveraging the dynamics of high-frequency oscillations and the non-linearity of fluid dynamics, both fluid elements and particles are forced on time-averaged steady trajectories, resulting in *streaming flow* and *particle migration*, respectively. A particularly well-developed way of obtaining vigorous rectification effects is driving a microbubble's interface at ultrasound frequencies. The resulting net flow, known generically as steady streaming [4], or, in this particular case, *microbubble streaming*, will advect solid particles placed in the flow volume. However, the particles will not necessarily behave as passive tracers, but will typically migrate onto specific trajectories and positions, and/or become *entrapped* in certain areas in the bubble's vicinity.

One of the first observations of such an entrapment was by Miller, Nyborg and Whitcomb [5]. They observed how human platelets formed aggregates around gas-filled micropores when the liquid was exposed to ultrasound. In a follow-up work, Miller [6] concluded that attractive acoustic radiation forces generated from the bubble's oscillation could not explain the experimental observations. Nonetheless, their discovery opened the door for new methods to trap, suspend, manipulate and even shear particles or cells of any kind, including motile cells. In recent years, with the development of microfabrication technologies and controlled microfluidic experiments, Lutz *et al.* [7] and Lieu *et al.* [8] generated microvortices – or *microeddies* – around solid microcylinders by imposing low-frequency liquid oscillations, showing the ability to trap sufficiently large particles. Marmottant and Hilgenfeldt [9, 10] proved that microvortices generated by the oscillation of sessile microbubbles – stabilized in micropores – can generate shear stresses capable of breaking up vesicles and cell membranes. That feature gives hydrodynamic manipulation through microbubble oscillations an advantage against competing micro-trapping techniques as optical trapping [2] or dielectrophoretic trapping [11].

Despite this technical progress, the physical mechanism behind the particle trapping phenomenon observed by Miller *et al.* [5, 6] remains unclear. Although the low-frequency trapping results of Lutz *et al.* [7] and Lieu *et al.*[8] showed trapping was possible even when acoustic radiation was negligible, subsequent by Rogers and Neild [12] and Chen *et al.* [13] proposed to model such trapping around larger oscillating bubbles using concepts of radiation force. Other authors [14, 15] have focused on a more direct numerical computation of inertial effects due to the finite size and density contrast of the particles in the streaming flow. In recent work, Agarwal *et al.* [16] presented an analytical treatment that showed how particle attraction to or repulsion from an oscillating bubble can indeed be described as a consequence of inertial effects dependent on the driving conditions as well as the particle and fluid properties. Acoustic radiation forces are incorporated into this formalism as a special case.

The controlled experiments in the abovementioned publications were almost exclusively designed to confine particle motion to a plane for easier quantification. However, Marin *et al.* [17] recently revealed the strong three-dimensional character of such streaming flows precisely due to the confinement in the third dimension. The acoustically-driven streaming flow around

semi-cylindrical bubbles analyzed in that work was theoretically described by Rallabandi *et al.* [18] using an asymptotic model reproducing the 3D particle trajectories. Although Marin *et al.*'s experiments were performed using finite-size particles (2-µm-diameter particles), considering the good comparison with the computed streamlines, it can be concluded that such small particles followed the streamlines faithfully and could be considered as passive flow tracers.

Going beyond the flow description, the aim of the current work is to examine and describe the size-sensitive migration and trapping of particles in such a 3D bubble streaming flow, and to understand how to make use of the 3D structure to separate particles along qualitatively different paths. Due to the intrinsic three-dimensional character of the particle motion, classical two-dimensional measurements methods will fail to resolve the real particle trajectories. Instead, in this work we obtain three-dimensional particle trajectories using a defocusing-based particle tracking method (General Defocusing Particle Tracking) [19].

Using experiments and numerical simulations, we show that knowledge of the 3D flow field is important to explain and exploit the systematic migration and trapping of buoyancy-neutral (density-matched) particles. It is also shown that the effects of forces on particles are captured by steric constraints only, simplifying the modeling.

II. EXPERIMENTAL SETUP

A sketch of the experimental setup is shown in Fig. 1. The experiments were carried out in a Polydimethylsiloxane (PDMS) microchannel with a rectangular cross-section of 500 µm × 72 µm and a blind side channel with width $w = 90$ µm and depth $l = 350$ µm. The microchannel was fabricated using soft lithography [20] and bonded to a glass slide previously covered with a 1-mm-thick PDMS film in order to have all channel walls made of PDMS. The bonding was realized by functionalizing the surfaces with a corona plasma treater (Elveflow, France). Once the microchannel is filled with liquid, a bubble remains at the blind side channel forming a gas-liquid interface that protrudes into the main channel. The system can be *short-circuited* to stop the flow by connecting the inlet to the outlet with a 4-way valve (see Fig. 1) and the bubble size can be adjusted by controlling the static pressure of the liquid as described earlier [21, 22]. The experiments in this work were performed with a bubble of width 110 µm protruding 50 µm into the main channel. Note that as a consequence of the manufacturing process, the edges of the blind side pit are blunt resulting in a slightly wider bubble than the width of the blind side channel (see inset in Fig. 1).

The bubble oscillations are driven by a piezoelectric transducer of 1 mm thickness and a diameter of 10 mm (Physik Instrumente, Germany), attached to the glass slide with epoxy two-component glue. The structure and

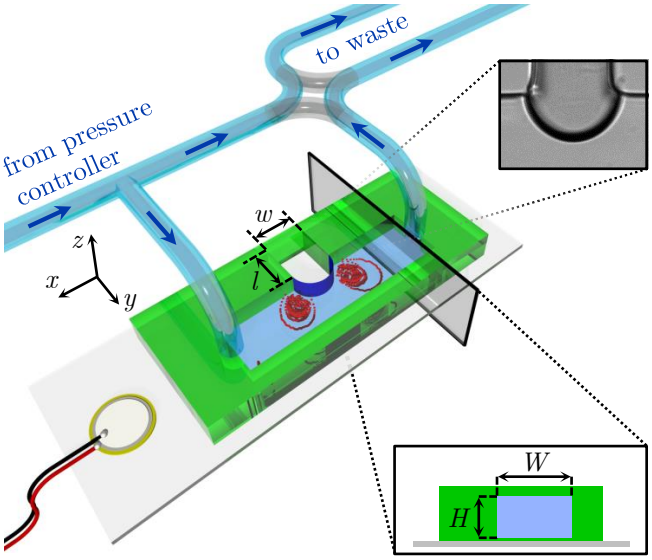

FIG. 1: Schematic (not in scale) experimental setup: A PDMS-microchannel with width $W = 500$ µm, height $H = 72$ µm, and total length of about 30 mm is filled with liquid and a sessile cylindrical bubble is formed in the blind side channel of width $w = 90$ µm and depth $l = 350$ µm. By switching the valve (indicated in grey), inlet and outlet of the microchannel are connected, leading to a uniform pressure in the system that stops the flow. The size of the bubble is controlled by adjusting the static pressure of the liquid with a pressure controller. By actuating the device with a Piezotransducer attached to the glass slide, surface oscillations are induced at the bubble interface generating a vortical acoustic streaming flow (in red) in the microchannel.

magnitude of the streaming flow generated by the bubble surface oscillation depends on the driving frequency and amplitude and the bubble size [22, 23]. For our investigation, we used an actuation frequency $f = 21.8$ kHz, a resonant frequency of bubble oscillation, with a peak to peak voltage $U_{pp} = 20$ V. The streaming flow generated with these settings was used to investigate the behavior of particles of different sizes dispersed in the fluid. In particular, we used fluorescent polystyrene spheres of diameter 2, 5, 10 and 15 µm (Microparticles GmbH, Germany) suspended in an aqueous glycerol solution with a glycerol content of 22.6% w-w to match the particle density [24].

The three dimensional particle trajectories were determined with General Defocusing Particle Tracking (GDPT) [19], a single-camera particle tracking method that uses pattern recognition to identify the depth position of spherical particles from the shape of their corresponding out-of-focus images. Astigmatic optics, consisting of a cylindrical lens placed in front of the camera sensor, was used to enhance the particle image deformation and extend the measurement volume [25, 26]. A high speed camera (PCO Dimax, Germany) was used to image the particles in fluorescent mode at frame rates around 300 fps and maximum exposure time. For this

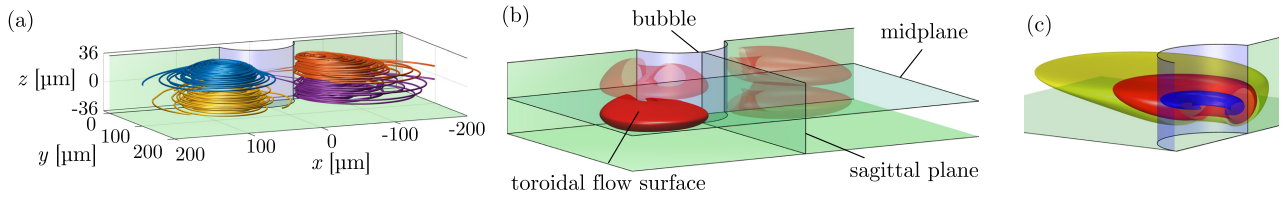

FIG. 2: Streaming flow close to the oscillating hemi-cylindrical microbubble. a) Trajectories of 2-µm-diameter particles. Plot shows one trajectory in each of the equivalent quadrants. b) Sketch of the flow structures and symmetry planes as observed in experimental investigations. The flow field is set up by four toroidal flow structures. These structures are symmetric to the midplane which is spanned in xy-direction at the midplane $z = 0$ and the sagittal plane at $x = 0$ which is spanned in yz-direction. c) A reconstruction of three toroidal flow surfaces from particle trajectories reveals the nested structure of these tori.

setup, we used a microscope objective of magnification 10× in combination with a cylindrical lens of focal length 500 mm, yielding a total measurement volume of approximately 2000 µm × 2000 µm × 100 µm, and an estimated uncertainty on the particle position of ∼ 0.5 µm in the xy-direction and ∼ 1 µm in the z-direction.

III. RESULTS

A. Flow structure around the bubble - Experiments

The flow structure around the bubble was investigated using tracer particles with a diameter of 2 µm, which can be considered as almost passive flow tracers. Fig. 2 a) shows the measured trajectories of four selected tracer particles which approximately follow streamlines of the fluid flow. In general, each particle trajectory is confined to one of the four regions defined by the two symmetry planes of the system: the midplane $z = 0$ and the sagittal plane $x = 0$. Away from the bubble, the particles move in almost planar trajectories ($z \approx$ const). But as they approach the bubble, the particles strongly accelerate and acquire a rapid motion along the z-axis, effectively "jumping" to a different z-position, with the direction and magnitude of the jumps depending on the loop size and position. Large loops pass closer to the bubble surface and their jumps move particles toward the midplane. Due to the symmetry of the flow, the loops also change along the bubble axis z: as the loops approach the midplane, they become tighter and more distant from the bubble surface. At a certain distance from the midplane, the drift in the z-direction is reversed, i.e., the particle appears to be reflected at the midplane, as it continues traveling towards the channel's top/bottom wall. A similar trajectory reflection occurs as a particle approaches the solid top/bottom walls. This pattern repeats itself over and over, with the trajectories lying on a torus-shaped surface as shown in Fig. 2 b). The trajectory of each tracer lies on the surface of a unique torus defined by its initial position. Tori of different sizes have a nested structure (as Russian nested dolls), with a small torus contained inside a larger torus as shown in Fig. 2 c). The innermost torus covers the smallest range of z and has negligible thickness, representing a single trajectory with we will call the *coreline* at a z-position $Z_{core} \approx \pm 18$µm. More details on these structures were revealed in previous work with experiments and simulations [17, 18].

Passive tracers will just travel along such nested structures. However, in the next section we show that finite-sized particles do not remain passive and describe how and why their trajectories deviate from the fluid pathlines described here.

B. Trajectories of differently sized particles - Experiments

Having described the structure of the streaming flow, we now focus on trajectories of 2-µm, 5-µm, 10-µm and 15-µm-diameter particles at time scales ranging from 3 to 30 seconds. Each experiments starts with particles at rest distributed randomly over the whole channel volume. When the ultrasound is turned on and the streaming flow is generated, particles are set into motion. Figure 3 shows the z-position of differently sized particles as a function of time. As can be seen in Fig. 3 a), 2-µm-diameter particles show a broad distribution within the z-range of the channel throughout the whole experiment. As mentioned in Section III A these particles seem to behave as passive tracers following the streamlines along certain toroidal flow surface given by the particle initial position. The length and amplitude of the continuous up and down movement in z therefore depends on the specific toroidal flow surface. However, looking carefully at the trend at longer times, one observes a narrowing of the z-range that the particle reaches. Ultimately particles migrate towards inner flow surfaces, i.e., torii of smaller extent in z. Therefore, the particle distribution in z at the end of the experiment tends to be concentrated at the coreline around $Z_{core} \approx \pm 18$ µm (see Fig. 3 a). This effect is stronger as particle size increases: 5-µm-diameter particles show a faster and more pronounced migration (Fig. 3 b). When these particles pass the perigee (location clos-

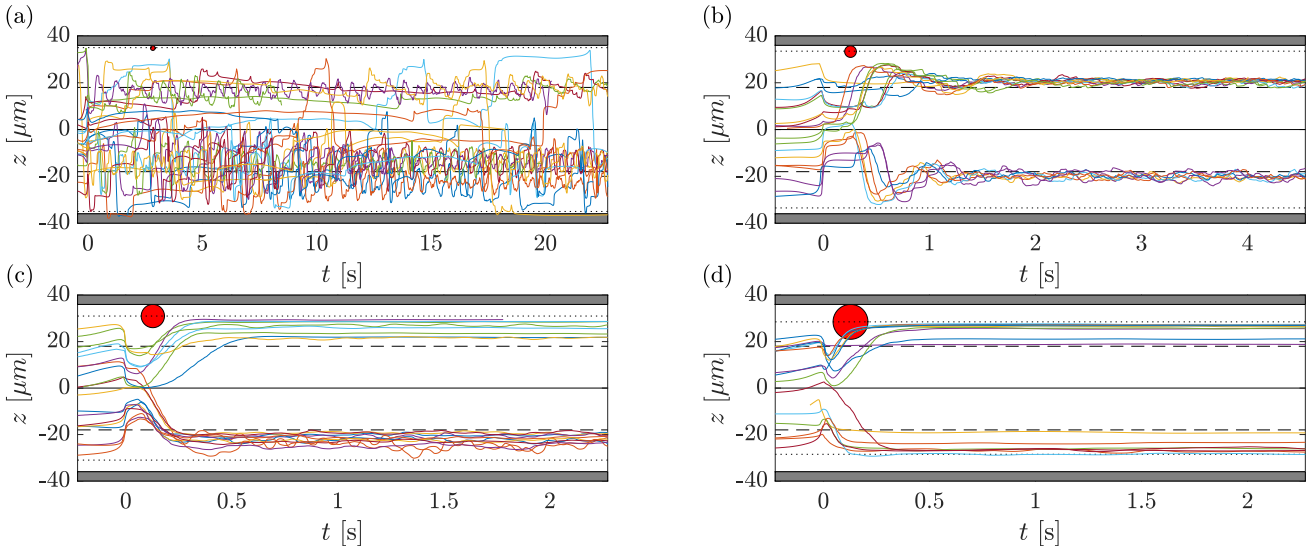

FIG. 3: Experimentally determined z-position of 2, 5, 10, and 15-µm-diameter particles in microbubble streaming flow as a function of time. After the particles pass the perigee for the first time (closest position to the bubble's interface, set to $t = 0$), they tend to migrate to a certain z-position at different rates depending on their size. Dashed lines depict the coreline at $Z_{core} \approx 18\,\mu m$. A red circle illustrates the size of the particle and dotted lines are drawn at one particle radius from the top and bottom walls. **a)** z-position for 2-µm-diameter particles: Particles slowly migrate towards inner tori of the flow structure. Focusing at a defined z-position is not observed. **b)** z-position for 5-µm-diameter particles: migration occurs within ∼1 second towards $Z_{core} = 18\,\mu m$ and $Z_{core} = -18\,\mu m$. **c)** z-position for 10-µm-diameter particles: migration occurs within ∼0.3 seconds. Particles focus at different z-Positions. **d)** z-position for 15-µm-diameter particles: migration occurs within ∼0.3 seconds. Particles primarily focus at the top and bottom walls of the microchannel. Dashed line: midplane; dotted lines: closest position of the particle center to top and bottom walls.

est to the bubble surface), they get displaced towards the eye of a toroidal flow surface. Within $\approx 1\,s$ the particle is stabilized near Z_{core}.

Although the migration process is similar at first glance for larger particles, the final z-position deviates from Z_{core} if the particle diameter is $d_p \gtrsim 10\,\mu m$: these larger particles migrate to positions closer to the top or bottom walls. That is the case for the larger particle sizes explored: 10-µm-diameter particles (Fig. 3c) and 15-µm-diameter particles (Fig. 3d). This is very clearly shown for 15-µm-diameter particles which, after migrating to the eye of the toroidal flow vortex, almost all end up in contact with either the top or bottom channel wall. Looking back at 10-µm-diameter particles, they seem to represent a kind of transition between a regime where particles are trapped at small central loops within the confinement volume (5-µm-diameter particles, Fig. 3b) and a regime where particles are trapped nearly touching the channel walls (15-µm-diameter particles, Fig. 3d). In order to get a deeper understanding on the processes that lead to the observed particle trajectories a simulation of the problem has been implemented that will be discussed in the following.

C. Trajectories of differently sized particles - Numerical model

As shown by Rallabandi *et al.* [18], the complex flow structure described above can be reproduced by a superposition of three streaming flow functions. Each function or mode satisfies the appropriate conditions in each of the three main planes: the bubble plane, the ceiling and

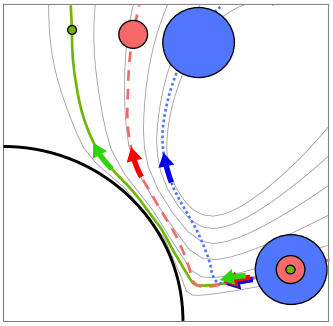

FIG. 4: Schematic of the steric interaction model for the simulation of trajectories of differently sized particles. While being advected in the streaming flow of the oscillating bubble, particles approach the bubble (black line) along streamlines (grey lines). A particle that would penetrate the bubble in a certain timestep of the simulation is radially displaced and forced to another streamline.

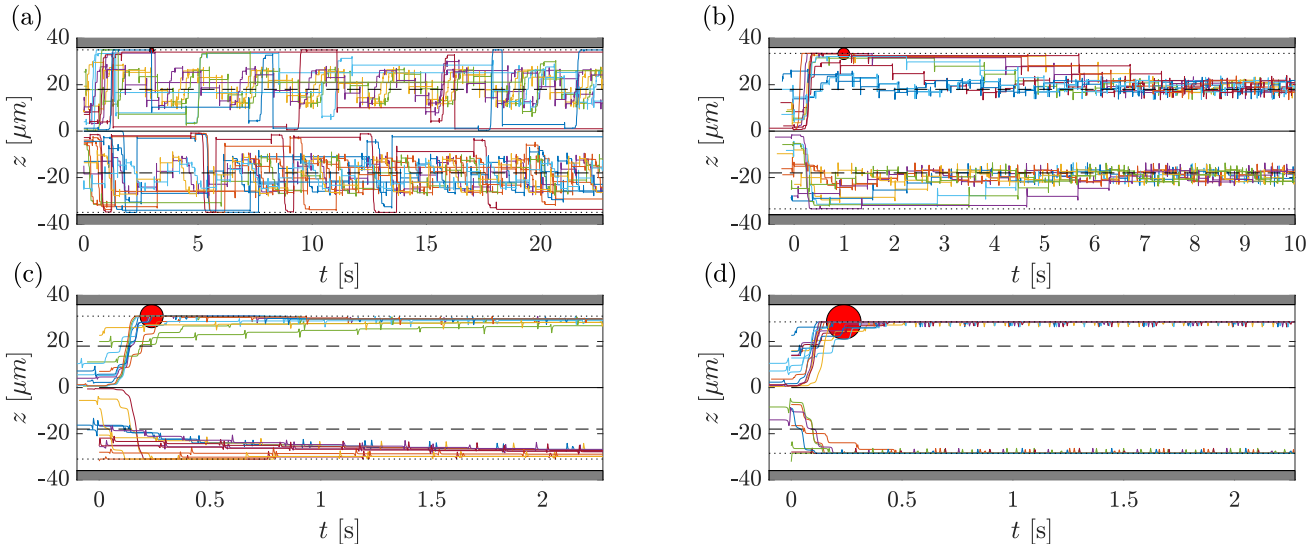

FIG. 5: Numerical z-positions of 2, 5, 10, and 15-µm-diameter particles in microbubble streaming flow as a function of the dimensionless time $\tilde{t}$. After the particles pass the perigee for the first time (closest position to the bubble's interface, set to $\tilde{t}$ =0), larger particles start to migrate to a certain z-position. Dashed lines depict the coreline at $Z_{core} \approx 18\,\mu$m. A red circle illustrates the size of the particle and dotted lines are drawn at one particle radius from the top and bottom walls.**a)** z-positions for 2-µm-diameter particles: Some particles slowly migrate towards inner torii of the flow structure, other particles span the whole volume of the microchannel. Focusing at a defined z-position is not observed. **b)** z-position for 5-µm-diameter particles: migration occurs before $\tilde{t} \sim 400$ towards $z = 18\,\mu$m and $z = -18\,\mu$m. **c)** z-position for 10-µm-diameter particles: migration occurs within ~ 20. Particles focus at different z-positions in the proximity of the channel walls. **d)** z-position for 15-µm-diameter particles: migration occurs within ~ 20. Particles focus at the walls of the microchannel.

the side wall. Rallabandi *et al.* [18] and Marin *et al.* [17] showed that flow tracers follow the streamlines computed from such stream functions.

While the physical nature of inertial forces near oscillating bubbles has been elucidated recently [16, 27], these computations are elaborate and have only been rigorously developed for 1D and 2D flow trajectories. Fortunately, a simplified scheme has been developed before [28, 29], in which the inertial forces are replaced by steric repulsion only: When the trajectory of a finite-size particle approaches the bubble to within a particle radius, the particle position is displaced in a direction normal to the bubble surface such that particle-interface interpenetration is prevented over the next numerical integration step (see Fig. 4). This principle is easily extended to our 3D flows, applying the same type of displacement whenever the particle touches a side wall or the top/bottom wall of the channel. We acknowledge that a proper description of particle motion in a flow like this involves more sophisticated modeling of rectified forces. However the dominant effect on particles close to interfaces has been found to be lubrication repulsion [27], which, due to its short range and strong magnitude, can be replaced by the steric hard-core force without great approximation.

The numerical model has been tested by introducing particles of different sizes at different initial positions in a systematic way. Time is normalized in the simulation by making use of the circular frequency of the oscillation ω and the bubble's oscillation amplitude relative to its radius, which we denote as ϵ. In the simulations, time is cast in a dimensionless variable $\tilde{t} = \epsilon^2\omega t$, where $(\epsilon^2\omega)^{-1}$ represents the characteristic timescale for the streaming flow. The choice of ϵ determines the maximum flow velocity $|v_{max}| = \epsilon^2\omega a_b$, a value of $\epsilon = 0.05$ yields velocities in the order of 20 mm/s. The results are shown in Fig. 5, where one can observe a clear migration of finite-sized particles when the particle diameter is larger than 2 µm. For the numerical time range explored, small 2-µm-diameter particles seem to keep traveling in the same toroidal flow surfaces where they started, whereas larger 5-µm-diameter particles get displaced to streamsurfaces close to the coreline of the toroidal flow structure. When the particle diameter is increased to 10 µm and 15 µm, particles typically get trapped in the vicinity of the top/bottom walls.

Although the computed detailed particle trajectories differs from the experimental one, Fig. 5 shows a good comparison in time scales and in final position for almost all particle sizes explored. In order to make a more quantitative comparison between experiments and simulations, we compute the final position of particles different sizes in the range 0.1 μm to 20 μm, with initial positions homogeneously distributed along the whole numerical volume. The computed final position Z_{end} is plotted as a function of the particle size and shown in Fig. 6. For a given particle size, we generally obtain a range of Z_{end} corresponding to a range of possible particle trajectories. Experimental results are shown as the mean of the final

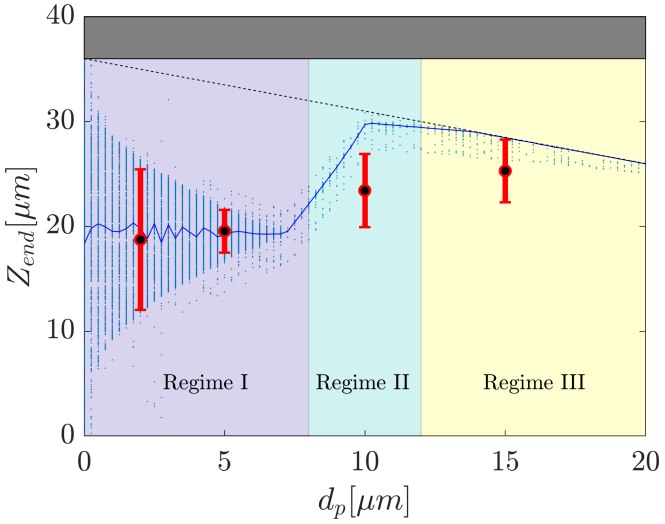

FIG. 6: Final particle positions Z_{end} as a function of particle diameter d_p. Red square markers show the average Z_{end} for experimental trajectories of a certain particle size and the red bar for the respective standard deviation value. Blue dots show Z_{end} for simulated particle trajectories and the blue line the respective mean values. PDMS channel is indicated in gray with a zone that particles can not enter due to their finite size (dotted black line). Due to the channel symmetry experimental results are mirrored to positive values at the midplane (black dashed line). Simulations trajectories for this figure were conducted only using initial particle positions with $z > 0$.

position and the error bar represents its standard deviation (24 trajectories for 2-µm-diameter particles, 19 for 5-µm-diameter particles, 19 for 10-µm-diameter particles and 16 for 15-µm-diameter particles). Fig. 6 shows a good match of the computed final particle location with those found in the experiments. It also shows three different regimes for different particle sizes that were already anticipated while analysing the experimental results. In regime I, particles do not migrate to a specific plane but remain on toroidal flow surfaces. As the particle diameter is increased, they are forced into inner flow surfaces. Therefore their Z_{end}-range decreases for increasing particle size until the particles tend to focus at the coreline at $Z_{end} \approx 18\,\mu$m, i.e. the smallest loops of the toroidal flow structure. Such a sharp focusing is already visible in the experimental data for 5-µm-diameter particles and it is clearly seen in the simulations. These particles have migrated towards the inner part of the nested toroidal flow structure by the steric interaction with the bubble. As the particle diameter is increased further $\gtrsim 7\,\mu$m, a different regime (II) appears and particles are forced into the flow at the eye of the toroidal structure, which moves towards the top/bottom wall of the microchannel [31]. The precise particle size above which migration towards top/bottom walls occurs seems to differ from the experiments, since experimentally not all $\sim 10\,\mu$m particles are fully migrated to the top wall, but remain trapped between the coreline and the top/bottom wall. The transition is nonetheless clearly represented in both the experimental data and the model.

Finally, above $d_p = 10$ µm all particles in the simulations and most particles in the experiments are trapped at a wall. Their only chance to escape is to follow streamlines passing close to the bubble interface, but their large size prohibits them from approaching close enough to the bubble to access these streamlines. Consequently, their position is so restricted that barely any motion is observed in the experiments in any direction.

A more quantitative description of the intermediate regime around 7 µm particle size may need to take into account the full range of rectified inertial forces identified in [16, 27], because (i) these forces are large for particles of $\gtrsim$ 10µm diameter. In particular, 10µm particles have have Stokes numbers of order unity, so inertial forces become significant. And because (ii) steric effects alone cannot confine the particles completely.

IV. DISCUSSION

We have shown that, by simply advecting finite-sized particles through a-priori known solutions for the steady streaming flow, one can obtain good quantitative agreement for the final migration position between experimental data and numerical results. Small particles can typically access any torii, but the amount of those available decreases as the particle size increases (regime I). A transition to regime II occurs, which is strongly dominated by particle-bubble steric interactions. Eventually, after a certain particle size, we enter in regime III, in which the only available positions are located in between the coreline and the top/bottom walls.

However, a few significant disagreements have been found: (1) 2-µm-diameter particles migrate slowly in experiments, while practically no migration is observed in the simulations. (2) The transitional regime II (Fig. 6) seems less pronounced in experiments than in simulations. (3) The ending position for larger particles (regime III in Fig. 6) is broader in experiments than in simulations. Several phenomena could be discussed to account for such discrepancies. Probably the most important effect that has not been considered so far would be the presence of inertial forces. Recent experiments with oscillating bubbles have shown the presence of rectified lift forces on particles [27, 29]. For example, it is clear that 2-µm-diameter particles would feel a significant lift force, which could explain why we observe certain migration in experiments and not in the simulations. The role of inertia becomes more important for larger particles, which might account for the discrepancies in regimes II and III (Fig. 6). It is however not the aim of this work to study in detail the role of the inertial forces in the long term migration of these particles. Also related to the presence of inertial forces is the effect of the flow velocity. In this study we have worked with maximum particle veloc-

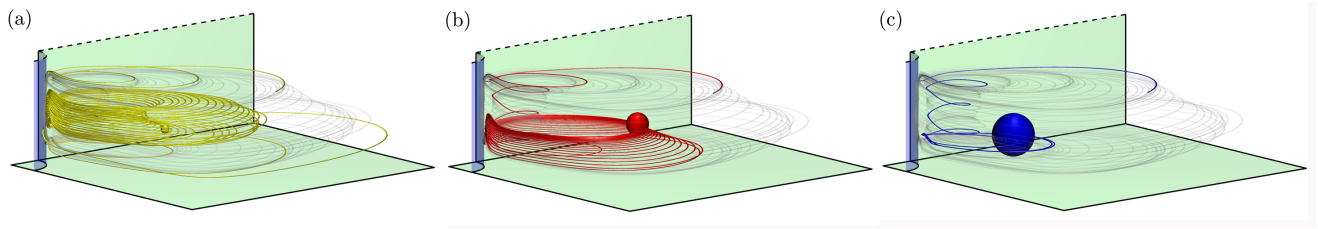

FIG. 7: Typical particle trajectories in the three regimes introduced in Fig. 6. Trajectories are calculated using the steric model described in Section III C. Spheres indicate final particle position and the particle size used for the simulation. (a) Typical trajectory of 3-µm-diameter particles (slow migration to small central loops).(b) Typical trajectory of 8-µm-diameter particles (faster migration to the central loops).(c) Typical trajectory of 15-µm-diameter particles (migration towards a wall).

ities (close to bubble) in the range of 20 mm/s (compatible with bubble amplitude of oscillations in the range of $\epsilon = 0.05$). Stronger actuation of the bubble might increase strongly inertial forces, even for the smallest particles studied here.

Although the particle concentration employed in each of the experiments is extremely low (less than 5 particles per image and per experiment), particle interactions could have occurred occasionally specially during the experiments with larger particles. Typically, in regime III (Fig. 6) two or three large particles could have perturbed each other, resulting in a wider distributions of positions.

Finally, another effect of crucial importance that has been avoided in this work is the role of buoyancy and particle-liquid density mismatch. All our results have been reproduced within a range of particle-to-fluid density ratio from 0.95 to 1.05 [32]. Larger or smaller density ratios might suffer from buoyancy, but also from different lift forces [30].

V. CONCLUSIONS AND FUTURE WORK

We have shown that the eventual fate of a particle introduced into a streaming flow can only be understood when taking into account the 3D flow structure, even in a case designed to emphasize 2D flow in a certain plane of the microchannel. Our quantitative experimental measurements and numerical simulations demonstrate that the migration of particles in the bubble's axial direction depends strongly and predictably on the particle size. While small enough particles behave as passive tracers and follow the streamlines [17, 18], larger particles migrate consistently, not only in the xy-plane, but also along the z-axis onto certain limiting trajectories in a very reproducible manner. The timescale of this migration depends strongly on the particle size and on the flow velocity, and very low influence has been observed for different density ratios.

Although a more careful study should include proper modeling of the inertial rectification forces known to act on the particles [14, 16, 27], our results show that a simple steric mechanism is sufficient to explain the size-selective and long-term migration observed in this bubble streaming scenario, and by extension in similar boundary-driven streaming flows.

Such three-dimensional particle migration should be very attractive for microfluidic devices for particle trapping and size-sensitive sorting applications. Our simple model could be a very useful tool to design different geometries in which particles of different sizes can be recovered and separated more efficiently.

Future work will be dedicated to understand the role of inertial forces in the long-term migration observed in these systems and to analyze the role of density mismatch.

Acknowledgements

Abundant discussions and technical help from Rune Barnkob and Raqeeb Thameem are greatly acknowledged. AV and CJK acknowledge financial support by the German Research Foundation grant KA 1808/17-1. AM acknowledges the European Research Council for support via the starting grant number 678573.

[1] L. Rayleigh, Philos. Trans. Roy. Soc. London Ser. A **175**, 1 (1883).
[2] A. Ashkin, Physical Review Letters **24**, 156 (1970).
[3] H. Bruus, J. Dual, J. Hawkes, M. Hill, T. Laurell, J. Nilsson, S. Radel, S. Sadhal, and M. Wiklund, Lab on a Chip **11**, 3579 (2011).
[4] N. Riley, Annual Review of Fluid Mechanics **33**, 43 (2001).
[5] D. L. Miller, W. L. Nyborg, and C. C. Whitcomb, Science **205**, 505 (1979).
[6] D. L. Miller, J. Acoust. Soc. Am. **84**, 1378 (1988).
[7] B. R. Lutz, J. Chen, and D. T. Schwartz, Anal. Chem. **78**, 5429 (2006).
[8] V. H. Lieu, T. A. House, and D. T. Schwartz, Analytical Chemistry **84**, 1963 (2012).
[9] P. Marmottant and S. Hilgenfeldt, Nature **423**, 153

(2003).
[10] A. Pommella, N. J. Brooks, J. M. Seddon, and V. Garbin, Scientific Reports **5**, 13163 (2015).
[11] X.-B. Wang, Y. Huang, P. R. Gascoyne, and F. F. Becker, IEEE Transactions on Industry Applications **33**, 660 (1997).
[12] P. Rogers and A. Neild, Lab Chip **11**, 3710 (2011).
[13] Y. Chen, Z. Fang, B. Merritt, D. Strack, J. Xu, and S. Lee, Lab Chip pp. 1–10 (2016).
[14] K. Chong, S. D. Kelly, S. Smith, and J. D. Eldredge, Physics of Fluids **25**, 033602 (2013).
[15] K. Chong, S. D. Kelly, S. T. Smith, and J. D. Eldredge, Physical Review E **93**, 013109 (2016).
[16] S. Agarwal, B. Rallabandi, and S. Hilgenfeldt, Physical Review Fluids **3**, 104201 (2018).
[17] A. Marin, M. Rossi, B. Rallabandi, C. Wang, S. Hilgenfeldt, and C. J. Kähler, Physical Review Applied **3**, 041001 (2015).
[18] B. Rallabandi, A. Marin, M. Rossi, C. J. Kähler, and S. Hilgenfeldt, Journal of Fluid Mechanics **777**, 408 (2015).
[19] R. Barnkob, C. J. Kahler, and M. Rossi, Lab on a Chip **15**, 3556 (2016).
[20] Y. Xia and G. M. Whitesides, Annual Review of Materials Science **28**, 153 (1998).
[21] A. Volk, M. Rossi, C. J. Kähler, S. Hilgenfeldt, and A. Marin, Lab on a Chip **15**, 4607 (2015).
[22] A. Volk and C. J. Kähler, Physical Review Applied **9**, 054015 (2018).
[23] C. Wang, B. Rallabandi, and S. Hilgenfeldt, Physics of Fluids **25**, 022002 (2013).
[24] A. Volk and C. J. Kähler, Experiments in Fluids **59**, 75 (2018).
[25] C. Cierpka, R. Segura, R. Hain, and C. J. Kähler, Measurement Science and Technology **21**, 045401 (2010).
[26] M. Rossi and C. J. Kähler, Experiments in Fluids **55**, 1809 (2014).
[27] R. Thameem, B. Rallabandi, and S. Hilgenfeldt, Physical Review Fluids **2**, 052001 (2017).
[28] C. Wang, S. V. Jalikop, and S. Hilgenfeldt, Biomicrofluidics **6**, 012801 (2012).
[29] R. Thameem, B. Rallabandi, and S. Hilgenfeldt, Biomicrofluidics **10**, 014124 (2016).
[30] S. Agarwal, B. Rallabandi, and S. Hilgenfeldt, Phys. Rev. Fluids **3**, 104201 (2018), URL `https://link.aps.org/doi/10.1103/PhysRevFluids.3.104201`.
[31] note that the system is symmetrical with respect to the channel midplane, and therefore the same discussion applies to the top and bottom walls.
[32] Assuming that our polystyrene particles have a density of 1.05 gr/cc, we have varied the water-glycerine solution density from 1 to 1.1 gr/cc.